

## Causal fracture prediction: curvature, stress, and geomechanics

LEE HUNT, SCOTT REYNOLDS, and SCOTT HADLEY, Fairborne Energy Ltd

JON DOWNTON, CGGVeritas

SATINDER CHOPRA, Arcis Corporation, Calgary, Alberta, Canada

We propose scaling volume curvature measurements with material property estimates to produce a superior prediction of natural fractures. Curvature is one of many, indirect, fracture-inferring attributes. It does not detect fractures, but is causally related to them through the assumption that increasing curvature relates to increasing strain. There are many other variables that are causally related to fractures. We propose that it would be advantageous to create combinations of these causal variables with curvature. Some of the most well known and important causes of variations in natural fracture density are material properties relating to brittleness. Material properties are critical geologically at all scales, from large-scale regional studies to prospect-level inquiries because the properties may vary significantly within individual formations and between formations. These vertical and lateral changes in material properties may be important and should be considered in fracture estimation, along with curvature. There is a lack of clarity regarding exactly which material property is best from the perspective of physics and rock mechanics; however, we have chosen a combination of parameters that we argue is a starting point. Fortunately, material properties are routinely estimated with amplitude variation with offset (AVO) techniques, and there is little practical reason not to use them together with curvature to produce a more complete attribute inferring fracture density. The combination of these variables is a step in the direction of creating quantitative causal fracture prediction estimates.

We consider different methods of combining curvature with material properties. This includes reference to the curvature-stress relationship instead of the commonly cited curvature-strain relationship, a change that suggests we should scale curvature with Young's modulus, or perhaps better, with an in-situ stiffness such as P-wave bound uniaxial modulus. We also considered the entire stress field by using a simplification of the in-situ bound closure stress equation to scale curvature. These methods have different levels of sophistication, which we show are inversely practical to implement. We tested the different approaches both qualitatively by evaluating the 3D surface seismic data volume characteristics and quantitatively by correlating to high-resolution electrical image log data recorded in West Central Alberta. We show that the use of any of our scaling methods is advantageous compared to only using curvature for fracture prediction. The use of more complex, geomechanically based means of scaling is desirable but has several challenges including the need for greater prior knowledge, and greater calibration data.

### West Central Alberta: different materials, different pressures

West Central Alberta has numerous clastic and carbonate targets. Much of the clastic section is gas-charged and overpres-

sured. Exploration targets include sandstones in the Cardium Viking, Notikewan, Rock Creek, and Nordegg formations. The entire section is structured, and reservoirs often exhibit structure and stratigraphic perseveration due to regional erosional surfaces (Boreen and Walker, 1991; Hunt et al., 2010b). There has been enough drilling, logging, and consequent production from these formations to identify some of the gross changes in material properties and pressure in the area. Figure 1 shows log and pressure data from a deep well in the area. This well was logged with gamma ray, bulk density, compressional velocity ( $V_p$ ), and shear velocity ( $V_s$ ). Lamé parameters rigidity ( $\mu$ ) and incompressibility ( $\lambda$ ) are calculated from these velocity logs. There are very clear and significant changes in these velocities and moduli at the Cardium, Viking, Rock Creek, Nordegg, and Elkton formation tops. These changes tell us that the rock properties are very different in these zones from the surrounding materials. The pressure data also depict sudden and significant changes with depth. The overburden pressure was calculated with the density log and depth data, while the pore-pressure curve is a model created from test data in the area. Rapid gross changes in pressure occur at certain shale-sandstone boundaries. The effective pressure curve is simply the difference between the overburden and pore pressures. It shows significant changes at the Cardium, Viking, Mannville, and Elkton interfaces. The Mannville section is particularly overpressured. Any of these changes in rock or material property, or in pressure, could have a strong affect on natural fracture density (Nelson, 2001) or in the ability to propagate fracture stimulations (Goodway et al, 2006).

### Curvature, stress, and strain

Curvature is defined as the rate of change of direction of a curve (Roberts, 2001). In its simplest form, curvature is described as the inverse to the radius of a circle that is tangent to the curve at a particular point. The measure can be made on any two- or three-dimensional surface, although the current state of the art relative to 3D seismic data is to calculate it volumetrically, based on dips calculated within the data itself rather than from an artificially picked horizon (Chopra and Marfurt, 2007).

As far back as 1968 (Murray, 1968), curvature has been related to fractures through the inference that greater curvature equates to greater strain. The strain of a folded layer has been described by Roberts (2001) and is reproduced in Figure 2. The layer shown has a thickness  $h$ . The curvature,  $K$ , is the inverse of the radius,  $R$ . The original length of the material was  $L_0$ . The top of the bed has length  $L_1$ , while the bottom of the bed has the length  $L_2$ . A neutral surface exists which experiences no stress and retains the original length  $L_0$ .  $L_1$  is greater than the original length  $L_0$ , which is greater than  $L_2$ , which means the top of the bed is experiencing extension, while the bottom of

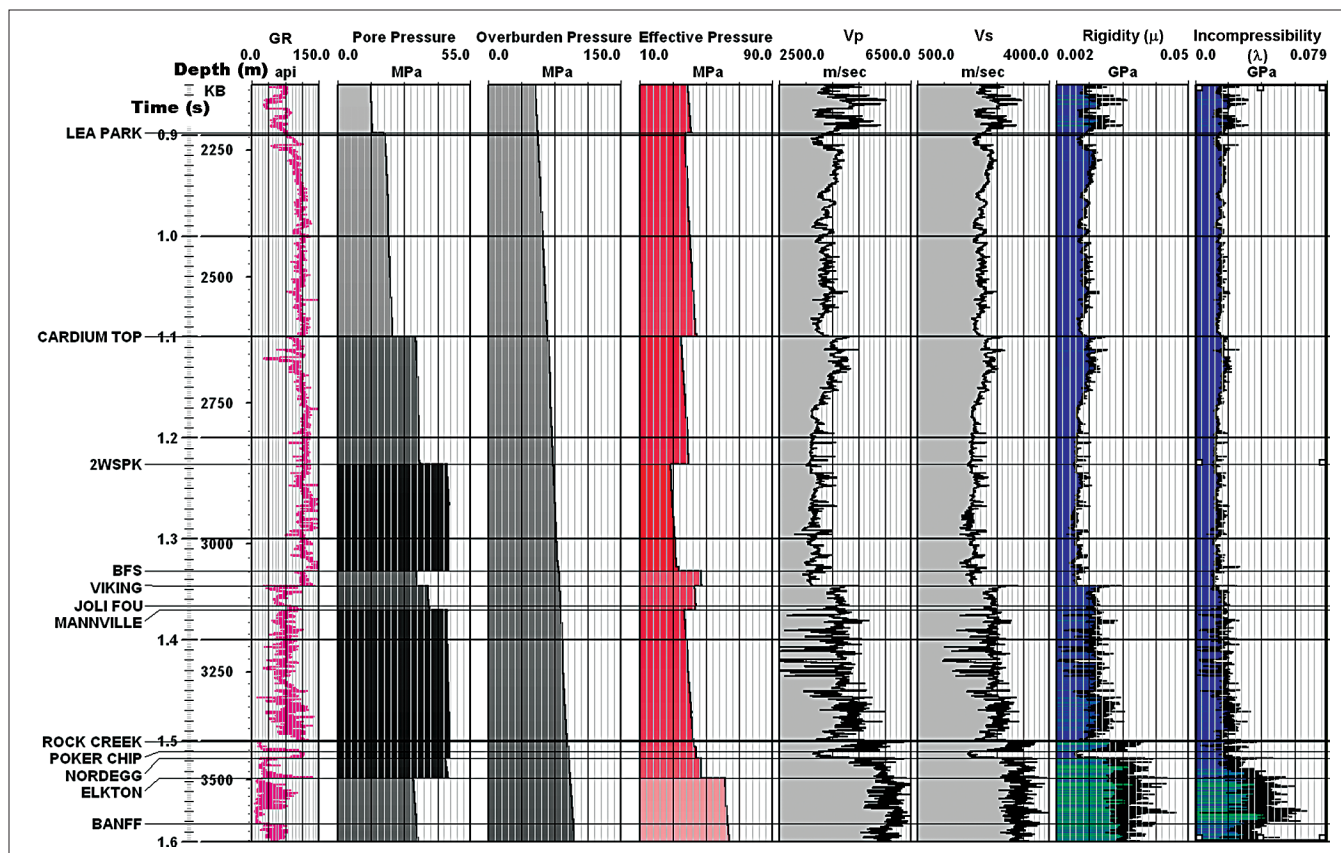


**Figure 1.** Deep well illustrating material properties and effective pressure changes with depth. Wireline logs include gamma ray, compressional velocity ( $V_p$ ), shear velocity ( $V_s$ ), rigidity ( $\mu$ ) and Lamé's first parameter,  $\lambda$ . The pore-pressure curve has major changes through the section illustrated. It was created from numerous production tests in the area, and has sharp changes at shale interfaces, consistent with those data. The velocity and Lamé parameter logs ( $\lambda$  and  $\mu$ ) show significant changes within the section as well, particularly at the Cardium, Viking, Rock Creek, Nordegg, and Elkton markers.

the layer is experiencing compression. The strain,  $e$ , at the top of this simple folded layer can be represented by the following expressions:

$e = (L_1 - L_0) / L_0$ , where  $e$  represents strain on the top of the layer (1)

$e = (h/2) / R = (h/2) * K$  where  $K$  represents the maximum curvature (2)

Hooke's law allows us to express the stress from this strain:

$\sigma = E e = E * (h/2) * K$ , where  $E$  represents Young's modulus (3)

This relationship also tells us that for a given curvature measure, the stress must increase with increasing Young's modulus.

$$e = \sigma / E = (h/2) * K \quad (4)$$

This implies that for materials prone to rupture rather than plastic deformation (brittle), large curvature and high Young's modulus values suggest very high stresses, and increasing probability of fracturing. Perez et al. (2011) suggest that we

should consider the fact that our seismic experiment involves in-situ rock that is bounded, unlike the single folded layer of Figure 2. This consideration results in the use of the bound Young's modulus ( $E_b$ ):

$$E_b = \lambda + 2\mu \quad (5)$$

The bound Young's modulus is simply the P-wave modulus (Perez et al., 2011).

These relationships suggest that we can use curvature to estimate both stress and strain in a layer. This information could then be used analytically to estimate strain, and then using Hooke's law and material properties, stress could be calculated. These values could then be calibrated to fracture density. Analytical calculations for stress and strain from curvature are not so easily done in practice. There are a variety of reasons why these relationships have not been used on seismic data. The first reason is that we almost never know the thickness of the layer being deformed. In fact, the deformed rock is likely a collection of different layers, and we may not easily define the top and base of the fold. To use curvature analytically, we also must recognize that the top of the bed is undergoing extensional forces, while the base is being compressed: fractures may be

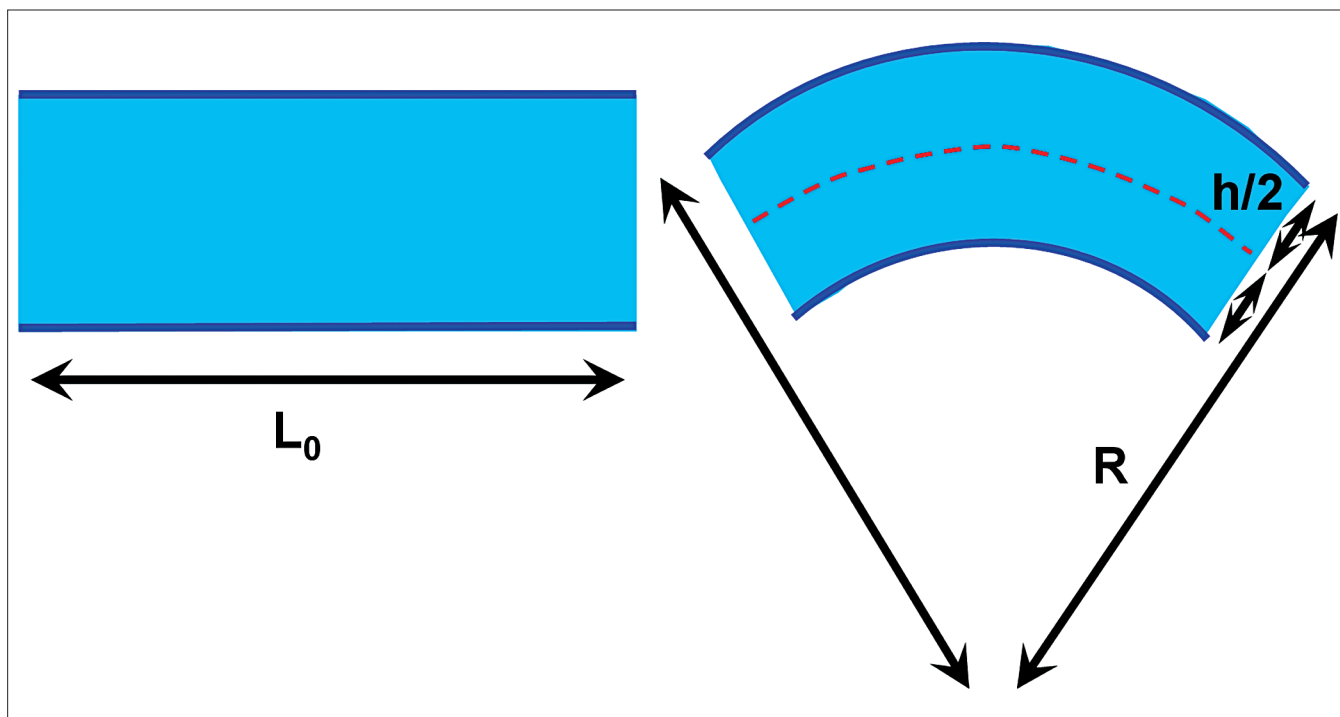


**Figure 2.** A single folded layer. The layer has a thickness,  $h$ . The curvature,  $K$ , is the inverse of the radius,  $R$ . The original length of the material was  $L_0$ . The top of the bed has length  $L_1$ , while the bottom of the bed has the length  $L_2$ . A neutral surface exists which experiences no stress and retains the original length  $L_0$ . Stress and strain can be calculated if we know the curvature, thickness, and Young's modulus of the layer.

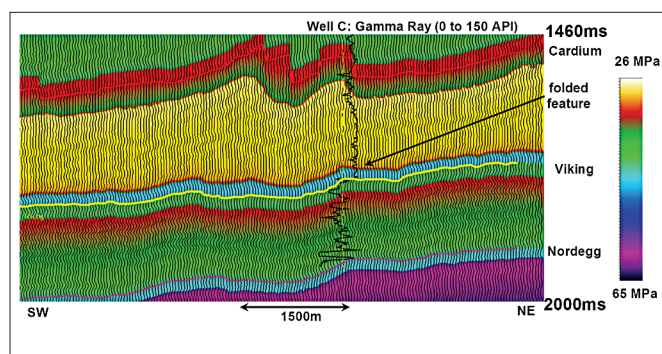


**Figure 3.** Pressure model based on production data. This model is horizon-consistent. A well with gamma-ray data is shown.

opened at the top and closed at the base. Moreover, in a compressive stress regime, the identification of extensional elements could be critical, as they may identify areas where overall stress is minimized and fracture stimulation behavior may change. It therefore follows that defining the thickness, top, and base, of the fold should be given serious attention. To our knowledge the consideration of layer thickness is not incorporated relative to seismic curvature measures. Such an endeavor may be achievable, but it will add an enormous complexity to the use of curvature. The second problem is that not all measured curvature is caused by folding or other tectonic deformation (Roberts, 2001); velocity effects as well as depositional or erosional structures can also cause apparent curvature features.

Despite these issues, curvature has been calibrated to frac-

Type	Parameter	Direction of correlation	Use both causes
Material Property	Rock brittleness	positive	
	Grain size	negative	
	Porosity	negative	
	Bed Thickness	negative	
In-Situ	Depth	variable effect	
	Pore Pressure	may hold fractures open	
Strain	Structural Position	positive with strain	

**Table 1:** Causes of fracture density variation.

ture density in a variety of settings. Keating and Fischer (2008) demonstrated that curvature bore an imperfect but definite relationship to actual strain measured in laboratory experiments with fault related folding. Hennings et al. (2000) demonstrated a strong correlation between total curvature and fracture intensity measured in outcrop. Hunt et al. (2010a) demonstrated statistically significant correlations between most-positive curvature from 3D seismic and fracture density in horizontal wells as validated by image-log data. These studies and others demonstrate that curvature is useful in estimating fracture density; however, none of the studies show anywhere near perfect correlations to the fracture density. How can we improve the curvature fracture inference?

### Many causes of fractures

There are two broad classes of fracture-prediction techniques:



direct, and indirect. Curvature is an indirect fracture estimator; nowhere in its formulation does it actually “see” fractures. The stress and strain relationship does not directly mean fractures exist, however, stress and strain are causes of fracturing. Nelson (2001) describes that there are many other causes of fracture density variations, which Hunt et al. (2009) summarized in a table, reproduced below as Table 1.

These causal variables are numerous, and have been exhaustively verified in the lab and in outcrop (Nelson, 2001). Dunphy and Campagna (2011) showed that the list of fracture causing variables is much more extensive than given in Table 1, is often unique to a particular fracture system, and can even be affected by different geologic facies with similar mineralogies. The applicability of curvature to infer variations in fracture density depends heavily on how much these other causes vary within a study area. Figure 1 demonstrated that the geology of West Central Alberta has tremendous changes in material properties and pressure. These changes are most obvious when viewed vertically, across stratigraphy, as in Figure 1; however, rock properties may also change laterally in the area as Hunt et al. (2010b) demonstrated in the Viking Formation. Since material and in-situ properties vary so profoundly in a vertical and lateral sense in this area, they should also be accounted for in any fracture inference that is interpreted from a consideration of causal factors. We are interested in finding a practical, physically meaningful way of combining these causes. Such a method should be called causal fracture prediction.

#### Strain-curvature or stress-curvature?

Rock brittleness is described ubiquitously in regards to fracture estimation, and is a key element to the assumed curvature-fracture relationship. Brittleness refers to a material that ruptures rather than plastically deforms once the stress exceeds its elastic limit. This stress value is referred to as the yield point and is often called the yield strength. When stresses are greater than the yield strength, fracturing will start to occur in a brittle material, although measuring exactly where inelastic deformation begins can be a point of some debate or controversy. There is no modulus that directly tells us what the yield strength of a material is, although Goodway et al. (2010) and Perez et al. (2011) discuss estimation of in-situ behavior and material strength from seismic data at length. Their work with the in-situ bound closure stress equation inspired some of the ideas to follow relative to that equation. Despite these efforts, material strength should still be measured in the laboratory under controlled conditions of temperature and pressure. This means that we have no simple and sure way of determining either yield strength or brittleness from seismic data. This being the case, we may still consider a practical strategy around at least considering brittleness as far as curvature goes.

We must consider carefully what we are trying to accomplish with this work: we are trying to make a practical im-

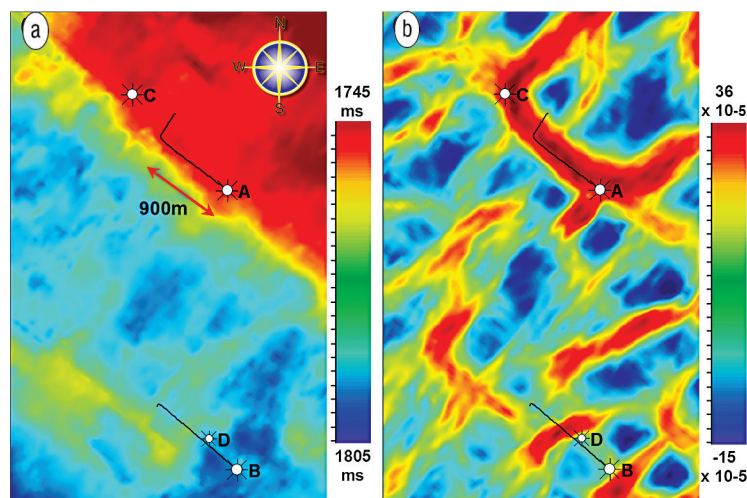


**Figure 4.** Maps illustrating structure and well positions. (a) Time structure map on the Viking. (b) The long-wavelength  $K_1$  curvature on the Viking. Much of the section, including the Nordeg, has similar structural characteristics.

provement to the use of curvature as a predictor of fractures. In the case of a folded structure comprised of many different rock types, we want to be able to discriminate which rocks may have higher fracture densities. We know from Nelson (2001) that materials such as dolomite and quartz sandstone fracture more readily in outcrop and in the laboratory than materials such as limestone and shale. These fracture-prone materials can be reasonably described as more brittle. They also have higher Young's modulus values. Hugman and Friedman (1979) demonstrated experimentally that decreasing grain size and porosity as well as increasing stiffness in mineral constituents acted to increase fracture density in carbonates. While we cannot say that Young's modulus measures brittleness perfectly for all materials, it appears to make a decent proxy for it in many observations of real geologic structures. We know from Hooke's law (Equation 3) that a rock of a given value of curvature must have a higher stress if Young's modulus is higher. We also know that all rock fails once it is subject to sufficient stress. For an unknown material, the higher the stress, the more likely it will fail. It follows that the high Young's modulus rock may therefore have a higher chance of failure and fracturing. Gray (2010) also recently suggested using Young's modulus to understand stress and brittleness in his work with azimuthal data. Nelson (2001) points out that fracture intensity in sedimentary rock is likely related to a combination of stress and strain, which also creates an argument to consider the curvature-stress relationship rather than the curvature-strain relationship. Therefore, we propose the following expression to scale curvature and create a more complete causal fracture predictor:

$$\begin{aligned} \text{Fracture density} \sim \text{Stress} &= E^*(b/2) K \text{ which simplifies to} \\ &\sim E^* K \end{aligned} \quad (6)$$

and again we lack knowledge of the bed thickness,  $b$ .

We call this causal fracture variable stress-curvature ( $EK$ ). Equation 6 suggests that our scaling of curvature to predict



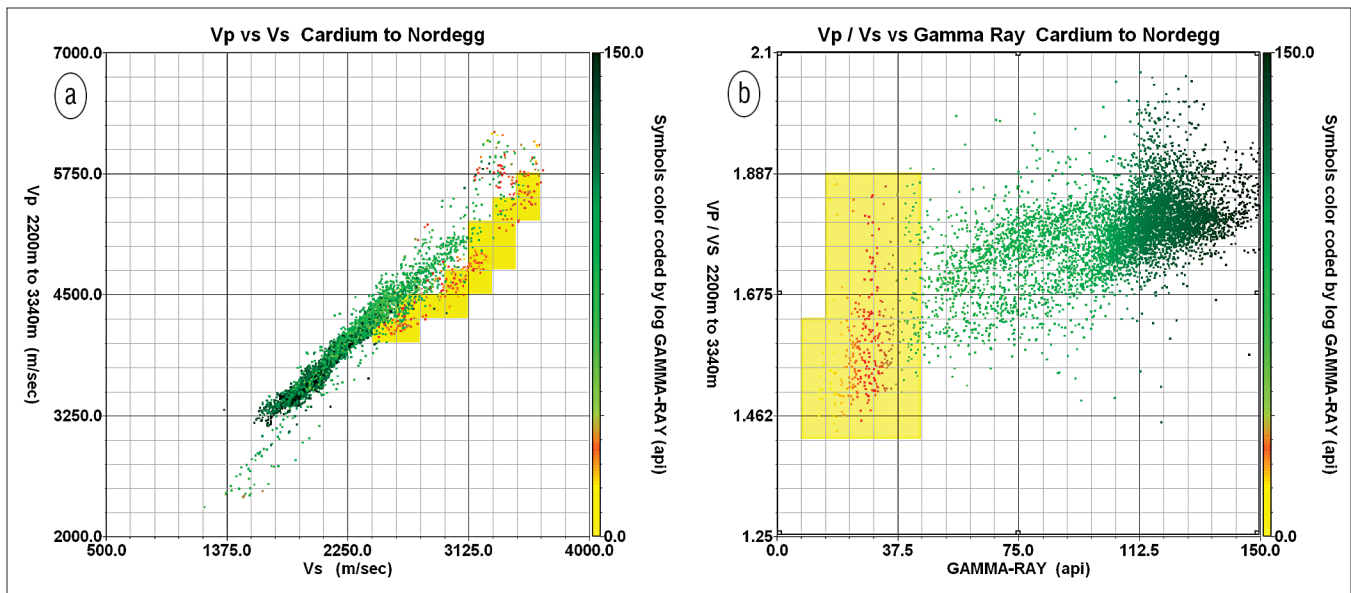


**Figure 5.**  $V_p$ ,  $V_s$ , and gamma-ray data relationships for well D. Areas with predominantly sandstone matrix are yellow, and the data points are colored with a gamma-ray-indexed color bar. (a)  $V_p$  versus  $V_s$  for the entire logged interval, including the Cardium to the Nordegg. It suggests a shale trend and a sand trend. (b)  $V_p/V_s$  versus gamma ray, showing there is a relationship between them.

natural fractures is simply taking a practical step toward estimating stress rather than strain.

Perez et al. (2011) suggest that we should consider that our use of Young's modulus in Equation 6 is only correct in unbound conditions. Moreover, Perez et al. (2011) and Goodway (personal communication) argue that the correct in-situ Young's modulus should be used. This notion yields a slightly different fracture density predictor:

$$\text{Fracture density} \sim \text{in-situ Stress} = E_b^* (b/2) K, \text{ simplifies to:} \\ \sim (\lambda + 2\mu) * K \quad (7)$$

We call this causal fracture variable bound stress-curvature ( $E_b K$ ).

### Closure stress

We may also refer to geomechanical theory in our consideration of how to combine material properties and curvature. In a triaxial regime where the maximum stress is vertical, the minimum horizontal stress is the minimum stress required to open a pre-existing plane of weakness. Goodway et al. (2006) rewrote the closure stress equation in geophysical terms:

$$\sigma_h = \lambda / (\lambda + 2\mu) [P_{\text{eff}} + 2\mu (\text{tectonic strain})] + B_H P_p \quad (8)$$

where  $\sigma_h$  is the minimum closure stress,  $\lambda$  is incompressibility,  $\mu$  is the rigidity,  $P_{\text{eff}}$  is the effective vertical pressure,  $B_H$  is the horizontal poroelastic constant, and  $P_p$  is the pore pressure. This equation does not directly tell us about fracture density; however, it relates the difficulty to hydraulically fracture a zone during a completion operation: lower values imply greater ease of fracture stimulation. Although the equation has a tectonic strain term, it does not easily lend itself to inclusion of the cur-

vature in the data, especially given the difficulties in determining whether curvature features are compressive or extensional, and what anisotropy they may have. Further to this, we expect to have greater density of natural fractures when stress and strain are higher (Nelson, 2001); while this equation refers to the minimum horizontal stress. Natural fractures and closure stress are not exactly the same two things. This concern can be brought to light in considering the effect of porosity on natural fracture density. Nelson (2001) shows that increasing porosity generally decreases fracture density, while Equation 8 suggests that increasing porosity (which would typically reduce the value of the  $\lambda/(\lambda + 2\mu)$  term) results in greater ease of fracture stimulation. This brings concerns about the possibility of misuse of this equation, and highlights potential differences between expectations of natural fracture density versus ease of fracture stimulation. Another assumption we make is that increasing values of curvature suggest the relief of tectonic stress through extension over folds. This is not true of all curvature measures, as stated earlier. We are using a convenient contradiction by saying that the extensional strain creates fractures, but also may relieve compressional tectonic strain (in Equation 8) and creates an environment where fracture stimulation could be easier to achieve. This contradiction is worse for curvature features with compressional strain. In these cases, there may well be natural fractures (which may or may not be closed), and the minimum closure stress may not be low at all. These possibilities are warnings of the oversimplification of this method, and suggest that even if we observe positive test results, the method cannot be universally applicable.

Nevertheless, let us examine Equation 8 further. Of particular interest is the  $\lambda/(\lambda + 2\mu) * P_{\text{eff}}$  term, which partially represents the amount of horizontal stress arising from effective vertical stress (Sayers, 2010). These terms should be accounted

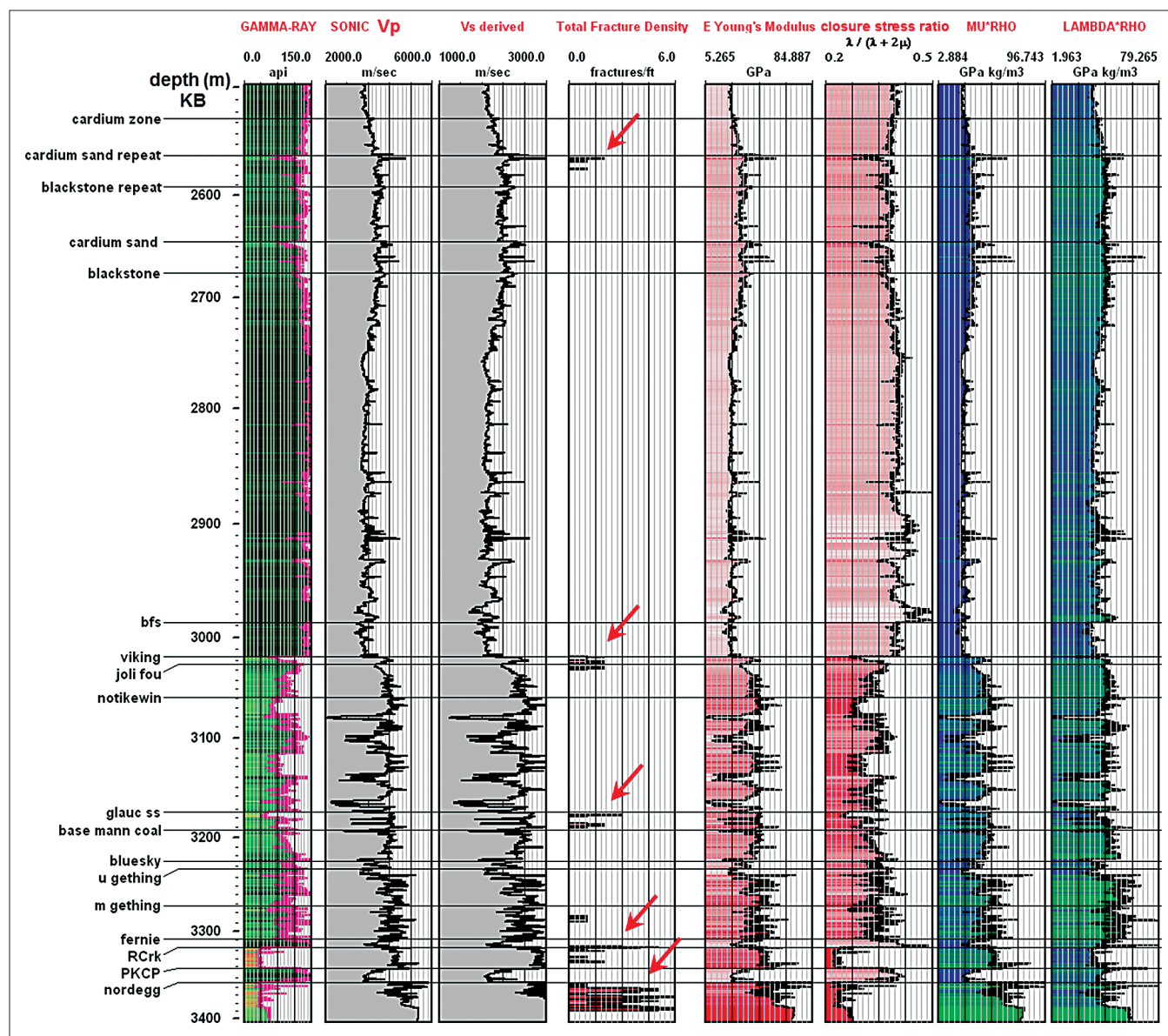


**Figure 6.** Well C log data, including estimated curves. The red arrows indicate areas where the fracture density is nonzero. In each case, the estimated Young's modulus is high and closure stress ratio is low.

for in our assessment of natural fracture density. Further, they are material and in-situ properties that we can estimate from seismic data.

We can estimate  $\lambda/(\lambda + 2\mu)$ , or CSR (Goodway, 2010), from seismic data with AVO analysis and inversion (Goodway et al., 1997). We could use this term to scale curvature as opposed to simply using Young's modulus as in Equations 6 or 7. Our closure-stress-related modifier to curvature can be simplified to the following expression:

$$\text{Fracture density} \sim \text{Strain estimate} / (\text{simplified difficulty to fracture}) \sim K * (\lambda + 2\mu) / \lambda \quad (9)$$

We call this causal fracture variable CSR-curvature ( $K/\text{CSR}$ ). Equations 7 and 9 will often have some similarities in behavior. The more dominant effect of incompressibility, or  $\lambda$ ,

in Equation 9 defines the difference between the closure stress approach versus the simpler Young's modulus approach to scaling curvature. Regardless of the approach taken, the proposed modifier to curvature have some similarity. Furthermore, estimating these parameters is commonly done and is practically achievable.

The estimate of  $P_{\text{eff}}$  from seismic is not as commonplace, but has still been adequately described in the literature. If we include the effective pressure term, and call the term material and in-situ property (MIP), our modification of curvature becomes:

$$\text{Fracture density} \sim \text{Strain estimate} / (\text{difficulty to fracture}) \sim K * (\lambda + 2\mu) / (\lambda * P_{\text{eff}}) \quad (10)$$

We call this causal fracture variable MIP-curvature ( $K/\text{MIP}$ ).



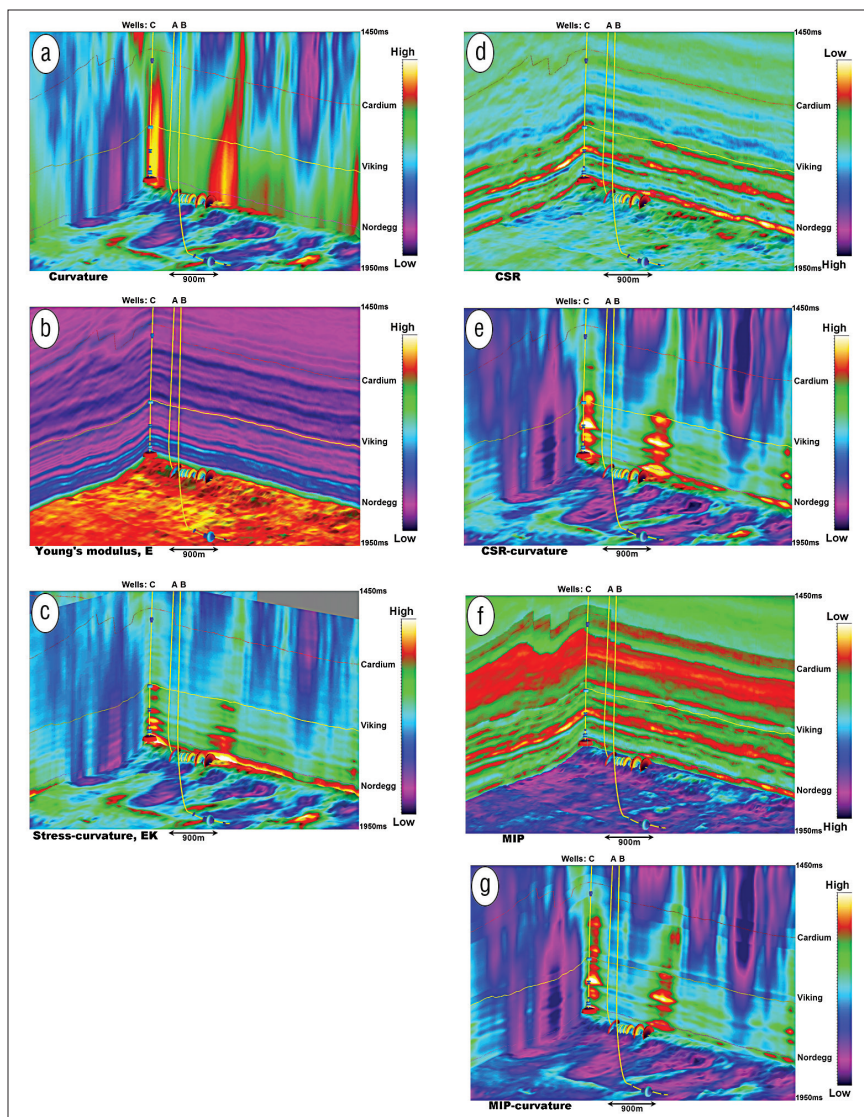


**Figure 7.** A chair diagram including wells A, B, and C with wells A and C in vertical section. The image log fracture-density data are displayed in cylinder form, with larger values of fracture density indicated with larger cylinder size and color changes from blue (small) to red (large). The horizon tops for the Cardium, Viking, and Nordegg are indicated. The values of each volume are colored according to size, and are indicated by color bars. (a) The long-wavelength  $K_1$  most-positive principal curvature. (b) The Young's modulus estimate. (c) The curvature scaled with Young's modulus, or stress-curvature. (d) The closure stress ratio, CSR. (e) CSR curvature. (f) The closure stress ratio times effective pressure (MIP). (g) MIP curvature

MIP). This formula may include effective pressure, but it still ignores the pore-pressure term at the end of Equation 8. In future work, the additional pore-pressure term could and perhaps should be included. For the sake of simplicity and practicality, we included only the pressure term that was coupled to the rock properties. Estimation of  $P_{eff}$  can be made in a variety of ways. In areas with sufficient drilling, production, and buildup data, a  $P_{eff}$  model could be built based solely on that prior knowledge. In areas where this is not the case, velocity methods of estimating  $P_{eff}$  may be attempted. Eaton (1975) and Bowers (1995) describe two velocity versus effective stress formulations that are commonly used. Gutierrez et al. (2006) and Sayers

(2010) discuss numerous other methods. Chopra and Huffman (2006) summarize some practical methods of implementation on 3D data. Changes in effective pressure have been estimated from 4D seismic experiments for some time (Tura and Lumley, 1999). Trani et al. (2011) summarized the 4D methods and extend them to include consideration of saturation changes as well as changes in effective pressure.

### Effective pressure models

Our study area has production from numerous zones, and with sufficient density that it is possible to build a simple effective pressure model from buildup data rather than the 3D velocity methods summarized by Sayers (2010) and Chopra and Huffman (2006). Figure 3 shows the pressure model created from the production data. This pressure model is consistent with the log curves shown in Figure 1. The horizon consistency of the model is considered to be of higher importance than lateral variations locally. The pressure varies remarkably from under- to significantly over-pressured. These data could be varied in a horizon consistent manner, which can vary by depth and according to lateral changes observed in other wells. The model we used was laterally invariant, and therefore extremely simplified. This simple approach still captures the essential changes in effective pressure, which are bounded by stratigraphic seals.

### A practical goal for causal fracture prediction

There may not be an approach to the causal fracture prediction problem that is both practical and physically perfect. While we should never accept the use of bad physics, we must also remember that even a flawed improvement we can produce today is sometimes better than the

dream of perfection in an imaginary tomorrow. The lack of a satisfactory measure of brittleness has the consequence that today's solutions are flawed and that we will certainly want further improvement tomorrow. This should encourage us on both counts rather than leave us afraid to make a mistake. In this work, we will test the ideas for scaling curvature against validation data from wells on a 3D seismic survey. Rather than dismiss any of the notions prematurely, we will simply test them all. Table II describes the various formulations we consider to scale curvature data and thereby create a causal fracture predictor. We expect that these scaling methods will yield similar results to each other.



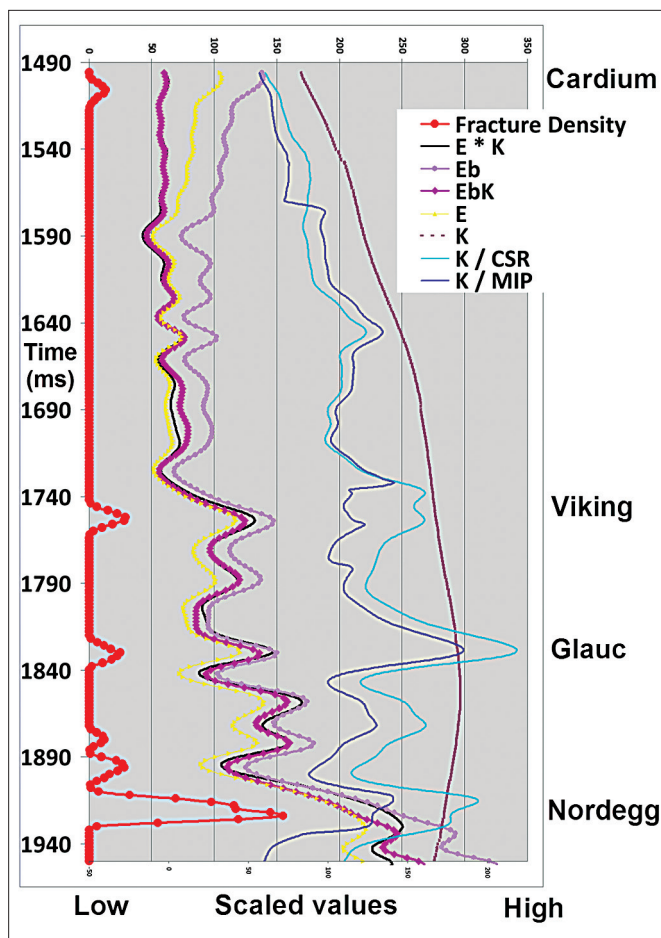


**Figure 8.** Image log fracture density and causal fracture attributes with time at well C. Each attribute is arbitrarily scaled with a constant for display purposes. The fracture swarms appear in the fracture density curve (red) at the Cardium (~1500 ms), the Viking (~1750 ms), the Glauconite (~1830 ms) and the Nordegg (~1920 ms). The curvature values change little in a vertical sense over this folded section. The Young's modulus curve (yellow) and the stress curvature (black) causal fracture predictor have the best apparent match to fracture density. The bound Young's modulus (purple) behaves almost exactly like the Young's modulus, and the bound stress-curvature (magenta) behaves almost exactly like stress curvature.

### Case study setup

We validated these results with well data from several reservoir zones. The validating data includes fracture-density data (high-resolution electrical image log) from two Nordegg horizontals, which was used by Hunt et al. (2010a) to investigate the ability of azimuthal methods and curvature to estimate fracture density. We also used a vertical well that had image log data spanning the Cardium through to the Nordegg zones. The observation of both vertical and lateral variations in material properties and fracture density is critical in this analysis. Although Hunt et al. (2010a) illustrated statistically significant correlations between curvature data and image log fracture density from two horizontal wells in the Nordegg, the calibration was only made for the Nordegg zone, and may not be valid for any other formation. As Figure 1 showed that there are major changes in effective pressure and rock properties by

## Do You Mind Your 2-D Gaps?



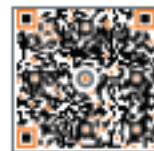
**Efficient Airborne Acquisition**  
Multi-measurement data at the basin scale with no boots on the ground

**Hydrocarbon Indicators**  
Nauyán Basin, Argentina

**neogeo.com**

NEOS can help. Our airborne sensor systems and proprietary interpretation platform allow you to integrate new geophysical measurements with your 2-D seismic data. So you can develop a 3-D understanding of what's happening between the lines. And make better decisions about where to lease and where to explore.

If you're thinking about filling in the white space, think **NEOS**.



**neos**  
Above, Below and Beyond

Name	Justification	Causal fracture density formula: scaling of curvature
Stress-curvature, (EK)	Hooke's law stress formulation	$E \times K$
Bound stress-curvature ( $E_b K$ )	Consideration of in-situ, bounded conditions	$(\lambda + 2\mu) \times K$
CSR-curvature, (K/CSR)	Closure stress ratio (CSR)	$((\lambda + 2\mu) / \lambda) \times K$
MIP-curvature, (K/MIP)	Closure stress $\times$ effective pressure (MIP)	$((\lambda + 2\mu) / (\lambda \times P_{eff})) \times K$

**Table 2:** curvature scaling methods to be tested

formation boundary, the calibration and correlation to vertical fracture density data should best illustrate the importance of the casual fracture method.

Figure 4 shows a map of the wells with the validation data. Figure 4a shows the time structure of the Viking. Figure 4b shows the long-wavelength K1 most-positive principal curvature (Chopra and Marfurt, 2010). Further reference to measured curvature in this paper will mean this particular type of curvature. The Mannville, Nordeg, and most of the shallow section have similar time structural and curvature characteristics. Wells A and B are the same well A and B from Hunt et al. (2010a). These wells have full log suites including  $V_p$ ,  $V_s$ , and image log fracture-density data. Well C is the vertical well with image log fracture-density data, density, gamma-ray, and compressional-velocity data. Well C lacks shear-velocity data. Well D is a nearby vertical well with both compressional- and shear-velocity logs, and is used to define  $V_p$  versus  $V_s$  relationships for well C. Wells A and C were drilled on a major folded feature that has high curvature values.

Figure 5 shows the relationships between  $V_p$ ,  $V_s$ , and gamma ray in well D. These data suggest that the  $V_p/V_s$  ratio is lower for sandstone dominated rock. We have observed this in many wells in the area, and interpret it as the gas effect being manifested in the more porous sandstone within the area. These data relationships were used to create a gamma-ray varying  $V_p/V_s$  ratio for well C. A  $V_s$  curve was estimated for well C using this varying  $V_p/V_s$  ratio. The estimation of this  $V_s$  curve was essential for illustrative purposes at well C. With the missing  $V_s$  estimated (even roughly, as in this case), Lamé's parameters curves, the closure stress ratio, and Young's modulus could all be estimated to accompany the all important image log fracture density data. More sophisticated methods of estimating  $V_s$  in well C were not necessary because the fit of  $V_p/V_s$  with other wells in the area was very good, and the illustrative use of the curve data did not require greater accuracy.

Figure 6 shows the log data for well C. The image log total fracture density has nonzero values only in specific places in the well: at the Cardium sand, Viking sand, Glauconite sand, Rock Creek sand, and Nordeg sand. These clusters of fractures are also where the estimated Young's modulus is high, and the closure stress ratio and lambda rho values are low. This is where we would expect the fracture density to be highest on a feature with consistent curvature.

### Results: data volumes

We validated these methods in three ways: by observations of the data volumes, by correlations of the attributes with the

fracture density data from the vertical well C, and by correlation of the attributes with the fracture density data from the horizontal wells A and B. Each method of validation is important, as they allow us to consider different things. The data volumes are important because they allow qualitative analysis to be conducted in time and space simultaneously. The vertical well analysis at well C takes place entirely in a curvature feature, and will be dominated by vertical or stratigraphic changes in rock properties. The horizontal wells are entirely in the Nordeg zone, and will have minimal changes in rock properties, but will sample lateral changes in curvature.

Figure 7 illustrates the important data volumes in the form of a chair diagram. An inline for each volume is intersected by a crossline such that they meet near well C. The crossline also runs along well A, which has the highest fracture density of the horizontal wells. A stratigraphic time slice of each data volume is also displayed, taken just under the Nordeg horizon. The fracture densities from the image logs are displayed as cylinders. Figure 7a shows the curvature volume. Well C is clearly in a curvature feature that persists vertically. Well A was drilled along the strike of the same curvature feature, while well B has relatively very minor curvature features, which are interpreted as being caused by strike-slip faulting. The lack of consideration of rock property changes is apparent in Figure 7a, especially in viewing the image-log fracture-density data of well C against the almost vertically invariant curvature at that location. The Young's modulus volume of Figure 7b does illustrate the stratigraphic rock property changes we expected to see based on our observations of the logs shown in Figure 1 and Figure 6. These changes are also illustrated in the CSR volume of Figure 7d. The values of Young's modulus and CSR change

Correlation coefficients ~450 ms	Up-scaled fracture density
Curvature (K)	0.195
Young's modulus (E)	0.734
Bound Young's Modulus ( $E_b$ )	0.715
Stress-curvature ( $E \times K$ )	0.674
Bound stress-curvature ( $E_b K$ )	0.644
CSR	-0.460
CSR-curvature (K / CSR)	0.420
MIP ( $CSR \times P_{eff}$ )	0.145
MIP-curvature (K / MIP)	0.228

**Table 3.** Correlation coefficients of the attributes versus the up scaled fracture density from the image log of vertical well C.



laterally in the displays, but those changes are relatively minor in comparison to their changes vertically, which we expected. Figure 7f illustrates the MIP volume, which considers the effective pressure model and CSR together. The various attempts at creating causal fracture volumes shown in Figures 7c, 7e, and 7g, all have gross similarities. Each volume is dominated laterally by curvature, and vertically by the rock properties being used. Each volume also has an apparent correlation with the vertical fracture-density variations displayed in well C.

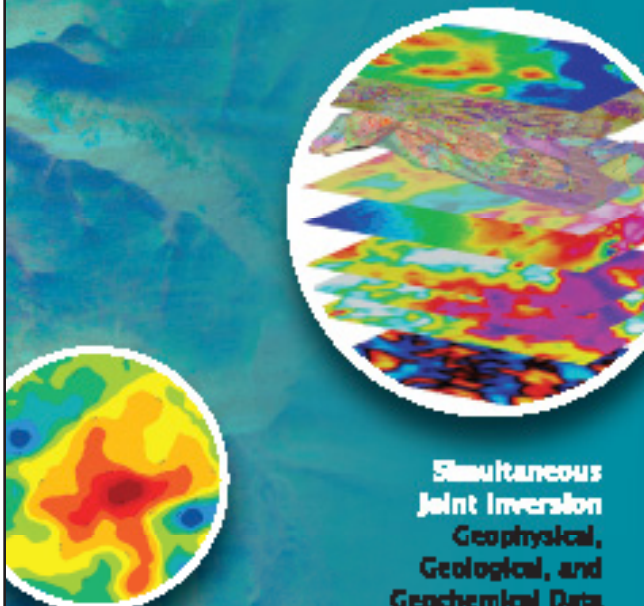
We do not show the bound Young's modulus or bound stress-curvature volumes because their appearance was almost identical to the unbound versions as shown in Figures 7b and 7c, respectively.

### Results: correlations

Our first quantitative comparisons are in a vertical sense at well C. We compare the upscaled image log fracture density and causal fracture attributes vertically at well C in Figure 8. The curvature is relatively invariant in a vertical sense over this folded section. In contrast, we know the rock properties change rapidly and significantly in vertical section. The Young's modulus curve (yellow) and the curvature times Young's modulus (stress-curvature) causal fracture predictor have the best apparent match to fracture density. The bound version of Young's modulus and stress curvature behaves almost exactly the same as the unbound versions in this data example. Curvature alone has a low correlation coefficient in a vertical sense. The curvature scaled by the closure stress ratio also has a good match to the fracture density, but the MIP scaling has the worst apparent match of the scaled curvature attributes. This could be due to small but important errors in the boundaries of the pressure model, or it could be due to the fact that we did not include all the pressure terms expected in Equation 8. This suggests that we may have to handle pressure more carefully and completely in order to use it to predictive advantage. We did not perform further tests with MIP curvature in this work as a consequence of this discouragement. Table 3 compiles the correlation coefficients between fracture density and these attributes. As Figure 8 suggests, Young's modulus and the stress-curvature variables (our causal fracture predictor) had the best correlation coefficients. The bound version of Young's modulus and stress curvature have very similar correlation coefficients as the unbound versions in this data example. The bound and unbound Young's modulus were so similar that we suspended comparing them further in this work. Curvature alone has a low correlation coefficient in a vertical sense. The CSR term has a statistically significant negative correlation coefficient to fracture density, which was expected. The correlation was not as high as the Young's modulus correlations. The MIP scaling yielded poor results.

We expected the vertical comparison to be dominated by the rock property changes, especially in a one-well comparison. This is due to the obvious fact that the entire section at well C is in a similar high curvature feature, but the lithology still changes vertically. In order to evaluate lateral changes in curvature, we must refer to the horizontal image log fracture-density data in wells A and B. We correlate the image-log data from

## Trying to Determine Where to Lease?




**Simultaneous  
Joint Inversion  
Geophysical,  
Geological, and  
Geochemical Data**


Gas Distribution  
Bosque-Haysville, USA

n e o s . c o m

**NEOS can help. Our airborne sensor systems and proprietary interpretation platform allow you to acquire and integrate all geophysical measurements with your seismic and well data. So you can map reservoir hydrocarbon saturations over broad areas. And make better decisions about where to lease and where to drill.**

**If you're thinking about where to lease, think NEOS.**







Correlation coefficients	Up-scaled fracture density
Curvature, (K)	0.628
Young's modulus, (E)	-0.669
Stress-curvature (EK)	0.566
CSR	-0.509
CSR-curvature (K / CSRP)	0.638

**Table 4.** Correlation coefficients of the attributes versus the up scaled fracture density from the image log data of Nordegg horizontal wells A and B from Hunt et al (2010a).

these wells to the attributes using the same methods of Hunt et al. (2010a). Table 4 compiles these correlation coefficients. These correlations are all statistically significant. In this case, curvature has a strong correlation to lateral variations in fracture density. Interestingly, Young's modulus also has a strong correlation to fracture density; however, it is a negative correlation. This is the opposite of the strong positive correlation that Young's modulus has with fracture density as estimated from vertical well C. The difference in sign is puzzling, is counter to our physical expectations, and the expectations from Nelson (2001). This contradiction suggests further scrutiny is required with additional validation data. The CSR is negatively correlated with fracture density for both the vertical and the horizontal wells, which is physically correct and more encouraging. In both the vertical and horizontal cases (Tables 3 and 4), the causal fracture variable created from curvature and CSR (K/CSR) improves over either variable alone. This lateral test is clearly dominated by curvature, while the vertical test was dominated by the changes in the rock itself. This makes the lateral test less indicative than the vertical test of the best causal fracture attribute.

Perspective on this effort requires that we consider all three of our validation methods. These combinations of variables are clearly encouraging when we consider the three-dimensional nature of our Earth as viewed in the volume displays, and the vertical and horizontal correlations. If we consider only one dimension in isolation, we may be persuaded that no combinations of variables are required, but by viewing the data in all three dimensions, we see the importance of considering these variables together.

### Conclusions and caveats

Predicting natural fractures from inference methods depends upon the completeness of the consideration of causal variables. We therefore believe that there is a predictive advantage to creating physically reasonable combinations of variables that are causally related to natural fractures. Curvature is a seismically available, important, fracture-inferring attribute. Material properties such as brittleness and in-situ properties should also be considered as they may strongly affect the likelihood of fracturing, and are commonly estimated from seismic. Unfortunately, measures of brittleness and failure of material do not have a simple modulus or measure that we can know exactly anywhere. This limitation forces us to consider a variety of methods to include these causal variables with curvature

to predict fractures. This included bound in-situ estimates of Young's modulus, which may represent a useful estimate of brittleness.

All of our attempts to combine curvature with other fracture-causing parameters are variations of the method of causal fracture prediction. Regardless of the rationale used, the scaling variables that we applied to curvature bore some similarity, and improved the overall fracture prediction accuracy. The simplest idea was to consider the curvature-stress relationship rather than the curvature-strain relationship. This approach suggested that curvature should be scaled by Young's modulus to predict fracture density. Using an in-situ bound expression for Young's modulus yielded little difference from the unbound expression in our data. Stress-curvature (or bound stress-curvature) yielded the best results of any method in our vertical well, but was somewhat inconsistent with the horizontal analysis. We recommend that the stress-curvature attribute be considered in fracture prediction studies. The contradictory results we observed for stress curvature between the vertical and lateral tests require further testing with additional validation data. Without additional testing, we cannot know if the problem was our validation data or an issue with the simplified physics of the approach. Since the vertical experiment was more dominated by material property changes (and had very little change in curvature) than the lateral experiment, which had very little change in material properties (but had significant changes in curvature), the stress-curvature scaling remains encouraging.

The CSR-curvature causal fracture variable came from consideration of the closure stress equation. The use of this equation seemed intuitively correct, although the relationship between ease of hydraulic fracture stimulation and natural fracture density is not entirely clear. The results of this approach were more consistent in both horizontal and vertical wells, and should also be considered in future work. In both of these approaches, the volumes appeared to match fracture densities in the vertical and lateral dimensions simultaneously. We must also consider that the CSR-curvature variable might be more suited to identifying ease of fracture stimulation than natural fracture density, although it was a good predictor of natural fractures in this experiment.

### Encouragement for future work

More complex means of scaling curvature that considered closure stress were also tested. This idea was implemented with only partial completeness. The use of the effective pressure term did not appear to be helpful in this example. We suspect that in order to better study the pressure effects, the use of all the pressure terms in the closure stress equation should be considered. This was not pursued exhaustively due to both scope and practical limitations. Further and more rigorous consideration of the stress field would be desirable.

Further work could also be done quantifying stress and strain from curvature by defining the top and base of each fold. We ignored the distance of the reservoir from the neutral surface in our assessment of stress and strain, which is a simplification used in all seismic curvature studies to date. This simplification is understandable, but may also be a crucial mistake

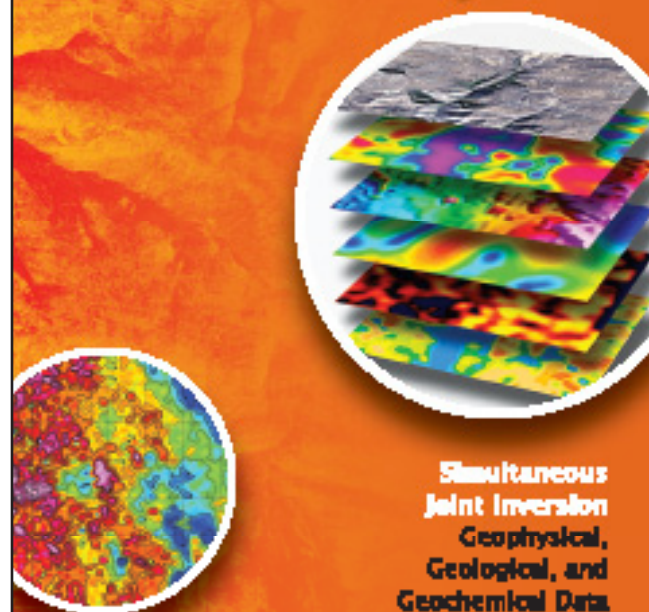
on all our parts, since that information is necessary to actually compute stress, and to tell us if that stress is extensional or compressional.

Other important fracture related parameters could be included, provided that they may be estimated in some way. There may be cases where additional geologic attributes such as facies could even be considered. As each fracture system has elements of uniqueness, the important causal parameters may not be perfectly known a priori, which suggests the need for careful consideration of all available information, and the possible requirement of even more sophisticated and physically rigorous causal fracture predicting formulations. **TLE**

## References

- Boreen, T., and R. G. Walker, 1991, Definition of allomembers and their facies assemblages in the Viking Formation, Willesden Green area, Alberta: *Bulletin of Canadian Petroleum Geology*, **39**, 123–144.
- Bowers, G. L., 1995, Pore pressure estimation from velocity data: Accounting for pore pressure mechanisms besides undercompaction: *SPE Drilling & Completion*, **10**, no. 2, 89–95, doi:10.2118/27488-PA.
- Chopra, S. and A. Huffman, 2006, Velocity determination for pore pressure prediction: *CSEG Recorder*, **31**, 28–46.
- Chopra, S. and K. J. Marfurt, 2007, Volumetric curvature attributes adding value to 3D seismic data interpretation: *The Leading Edge*, **26**, no. 7, 856–867, doi:10.1190/1.2756864.
- Chopra, S. and K. J. Marfurt, 2010, Integration of coherence and volumetric curvature images: *The Leading Edge*, **29**, no. 9, 1092–1107, doi:10.1190/1.3485770.
- Dunphy, R. and D. Campagna, 2011, Fractures, elastic moduli & stress: geologic controls on hydraulic fracture geometry in the Horn River Basin: *CSEG Convention, CSEG-CSPG-CWLS Convention Extended Abstracts*.
- Goodway, W., T. Chen, and J. Downton, 1997, Improved AVO fluid detection and lithology discrimination using Lamé petrophysical parameters; “ $\lambda\rho$ ”, “ $\mu\rho$ ”, & “ $\lambda/\mu$  fluid stack”, from P and S Inversions: 67th Annual International Meeting, SEG, Expanded Abstracts, 16, 183–186.
- Goodway, W., J. Varsek, and C. Abaco, 2006, Practical applications of P-wave AVO for unconventional gas resource plays-I: *CSEG Recorder*, 2006 Special Edition, 90–95.
- Gray, D., 2010, Targeting horizontal stresses and optimal hydraulic fracture locations through seismic data: 6th Annual Canadian Institute Shale Gas Conference, [http://www.cggveritas.com/technicalDocuments/cggv\\_0000006453.pdf](http://www.cggveritas.com/technicalDocuments/cggv_0000006453.pdf) Eaton, B. A., 1975, The equation for geopressure prediction from well logs: *SPE paper* 5544.
- Hennings, P. H., J. E. Olson, and L. B. Thompson, 2000, Combining outcrop data and three-dimensional structural models to characterize fractured reservoirs: An example from Wyoming: *AAPG Bulletin*, **84**, no. 6, 830–849.
- Hugman, R. H. H. III, and M. Friedman, 1979, Effect of Texture and composition on Mechanical Behavior of Experimentally Deformed Carbonate Rock: *AAPG Bulletin*, **63**, no. 9, 1478–1489.
- Hunt, L., S. Chopra, S. Reynolds, and S. Hadley, 2009, On calibrating curvature data to fracture density: causes: *CSEG Recorder*, **34**, 27–32.
- Hunt, L., S. Reynolds, T. Brown, S. Hadley, J. Downton, and S. Chopra, 2010a, Quantitative estimate of fracture density variations in the Nordegg with azimuthal AVO and curvature: A case study: *The Leading Edge*, **29**, no. 9, 1122–1137, doi:10.1190/1.3485773.
- Hunt, L., J. Downton, S. Reynolds, S. Hadley, D. Trad, and M.

# Fractures Driving Your Well Productivity?



Fracture Swarms  
Mesaona Basin, Colorado

Simultaneous  
Joint Inversion  
Geophysical,  
Geological, and  
Geochemical Data

neogeo.com

NEOS can help. Our airborne sensor systems and proprietary interpretation platform allow you to acquire and integrate all geophysical measurements with your seismic and well data. So you can map fracture fairways over broad areas. And make better decisions about where to lease and where to drill.

If you're thinking about fractures, think NEOS.



neogeo  
Above, Below and Beyond

- Hadley, 2010b, The effect of interpolation on imaging and AVO: A Viking case study: *Geophysics*, **75**, no. 6, WB265–WB274, doi:10.1190/1.3475390.
- Gutierrez, M. A., N. R. Braunsdorf, and B. A. Couzens, 2006, Calibration and ranking of pore-pressure prediction models: *The Leading Edge*, **25**, no. 12, 1516–1523, doi:10.1190/1.2405337.
- Keating, D. P. and M. P. Fischer, 2008, An experimental evaluation of the curvature-strain relation in fault-related folds: *AAPG Bulletin*, **92**, no. 7, 869–884, doi:10.1306/03060807111.
- Murray, G. H., 1968, Quantitative fracture study - Spanish Pool, McKenzie County, North Dakota: *AAPG Bulletin*, **52**, no. 1, 57–65.
- Nelson, R., 2001, *Geologic analysis of naturally fractured reservoirs*; Elsevier.
- Perez, M., D. Close, B. Goodway, and G. Purdue, 2011, Developing Templates for Integrating Quantitative Geophysics and Hydraulic Fracture Completions Data: Part I - Principles and Theory: 81st Annual International Meeting, SEG, Expanded Abstracts, 1794-1798.
- Roberts, A., 2001, Curvature attributes and their application to 3D interpreted horizons: *First Break*, **19**, no. 2, 85–99, doi:10.1046/j.0263-5046.2001.00142.x.
- Sayers, C. M., 2010, *Geophysics under stress: Geomechanical applications of seismic and borehole acoustic waves*: SEG.
- Tura, A., and D. E. Lumley, 1999, Estimating pressure and saturation changes from timelapse avo data: 69th Annual International Meeting, SEG, Expanded Abstracts, 1655–1658.
- Trani, M., R. Arts, O. Leeuwenburgh, and J. Brouwer, 2011, Estimation of changes in saturation and pressure from 4D seismic and AVO time shift analysis: *Geophysics*, **76**, no. 2, C1–C17, doi:10.1190/1.3549756.

*Acknowledgments: We thank Graham Carter of CGGVeritas, Bill Goodway of Apache Corporation, Dave Gray of Nexen Inc, and Doug Schmitt of the University of Alberta. We also thank Fairborne Energy Ltd and CGGVeritas Canada for permission to show this information.*

*Corresponding author: LHunt@fairborne-energy.com*